DNA Nanostructures Hot Paper

Deutsche Ausgabe: DOI: 10.1002/ange.201509772
Internationale Ausgabe: DOI: 10.1002/anie.201509772

Multiscale Origami Structures as Interface for Cells

*Alessandro Angelin, Simone Weigel, Ruben Garrecht, Rebecca Meyer, Jens Bauer, Ravi Kapoor Kumar, Michael Hirtz, and Christof M. Niemeyer**

Abstract: *A DNA-based platform was developed to address fundamental aspects of early stages of cell signaling in living cells. By site-directed sorting of differently encoded, protein-decorated DNA origami structures on DNA microarrays, we combine the advantages of the bottom-up self-assembly of protein–DNA nanostructures and top-down micropatterning of solid surfaces to create multiscale origami structures as interface for cells (MOSAIC). In a proof-of-principle, we use this technology to analyze the activation of epidermal growth factor (EGF) receptors in living MCF7 cells using DNA origami structures decorated on their surface with distinctive nanoscale arrangements of EGF ligand entities. MOSAIC holds the potential to present to adhered cells well-defined arrangements of ligands with full control over their number, stoichiometry, and precise nanoscale orientation. It therefore promises novel applications in the life sciences, which cannot be tackled by conventional technologies.*

Surface-based bioanalytical methods are of utmost importance for fundamental and applied biomedical research. For example, owing to the high degree of miniaturization and multiplexing capabilities, DNA[1] and protein microarrays,[2] or combinations thereof,[3] are widely applied in high-throughput assessment of biological processes. While the fabrication of such microarrays is usually conducted by so-called "top-down" methods, such as ink-jet and microcontact printing or (photo)lithography, to create micrometer-sized patterns of biomacromolecules, nanometer-sized arrays of molecules can be efficiently generated by "bottom-up" approaches, which take advantage of molecular self-assembly. As a prime example, Seeman's groundbreaking developments of "structural DNA nanotechnology"[4] and subsequent advancements through Rothemund's scaffolded origami technique[5] have made available a large repertoire of methodologies for the ready access of well-defined nanometer-sized scaffolds. Importantly, these can be used as molecular pegboards for the precise arrangement of proteins or other components with a lateral resolution of approximately six nanometers.[6] This structuring capability would be tremendously useful for bioanalytical applications, which address native biomolecular assemblies of similar size, such as the supramolecular clusters of tens to thousands of membrane-associated molecules found in the membrane of living cells. These typically reveal ultrastructural features in the regime of five to hundreds of nanometers and are assumed to play a crucial role in the final outcome of signaling events and thus the development of the cellular phenotype.[7] While it seems possible to address these biological phenomena with designed DNA architecture, the implementation of protein-decorated DNA origami structures into surface-based techniques is currently not well developed.

DNA origami nanostructures have been patterned by adsorption onto chemically modified[8] or lithographically structured[9] solid supports and onto lipid bilayer membranes.[10] However, to take full advantage of the multiplexing capabilities of surface-based analytical methods, the site-directed immobilization and sorting of sets of differently encoded, protein-decorated DNA origami structures on suitably patterned surfaces would be required. We here report the development of MOSAIC (multiscale origami structures as interfaces for cells), an innovative DNA-based platform which combines top-down micropatterning of surfaces and the bottom-up assembly of nanoscaled protein arrangements for the investigation of membrane-associated processes in living cells. To gain control over the spatial orientation of protein-decorated origami nanostructures with respect to the solid substrate, we used origami constructs with single-stranded tags to facilitate their site-directed sorting on surface patterns encoded with a set of complementary DNA oligonucleotides (Figure 1). The resulting patterns provide stable interfaces for cell culturing. Using origami constructs presenting the epidermal growth factor (EGF) as ligand for the cellular epidermal growth factor receptor (EGFR), we demonstrate that the nanoscaled architecture of this MOSAIC system specifically affects EGFR activation in adhered MCF7 cells.

To establish the site-directed sorting of origami nanostructures on microarrays (Figure 1 A,B), we designed $54 \times 91\ nm^2$ rectangular origami constructs from the 5438 nt template 109Z5 (nt = nucleotide),[11] which are equipped with nine single-stranded DNA (ssDNA) binding tags, protruding from one side of the plane of the quasi-2D nanostructure (details of the origami design and a full list of oligonucleotide sequences are given in the Supporting Information). The binding tags' 22-mer coding sequence was appended to the origami rectangle through a dT_8 spacer sequence (Figure 1 C). We chose three different previously

[*] A. Angelin, S. Weigel, R. Garrecht, Dr. R. Meyer, J. Bauer, Prof. Dr. C. M. Niemeyer
Karlsruhe Institute of Technology (KIT)
Institute for Biological Interfaces (IBG 1)
Hermann-von-Helmholtz-Platz
76344 Eggenstein-Leopoldshafen (Germany)
E-mail: niemeyer@kit.edu
R. K. Kumar, Dr. M. Hirtz
Karlsruhe Institute of Technology (KIT)
Institute for Nanotechnology (INT) &
Karlsruhe Nano Micro Facility (KNMF)
Hermann-von-Helmholtz-Platz
76344 Eggenstein-Leopoldshafen (Germany)

Supporting information for this article is available on the WWW under http://dx.doi.org/10.1002/anie.201509772.

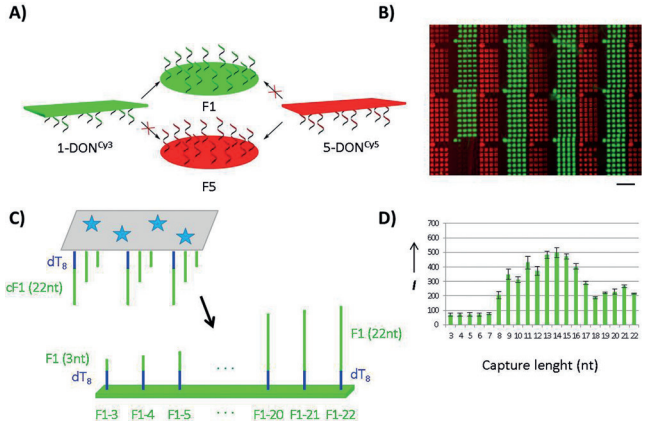

Figure 1. Site-directed sorting of DNA origami nanostructures on microarrays. A) Schematic illustration of origami sorting through specific hybridization with surface-bound complementary capture oligonucleotides. A mixture of two different origami constructs, **1-DON^{Cy3}** and **5-DON^{Cy5}**, labeled with Cy3- (green) or Cy5- (red) modified staple strands and containing either the cF1 or the cF5 single-stranded DNA (ssDNA) binding sides protruding from the rectangular structure of the origami construct, respectively, bind to their complementary, surface-bound capture oligonucleotides F1 (green) and F5 (red), respectively. The fluorescence image in B) shows a representative result of this experiment (scale bar = 50 μm). The influence of the length of the ssDNA binding tags on the hybridization efficacy was investigated with an array of capture oligomers of different lengths. The schematic illustration and obtained signal intensities are shown in (C) and (D), respectively (see text for details).

optimized oligonucleotide sequences (cF1, cF5, cF10)[12] for the binding tags to encode the three different DNA origami nanostructures **1-DON**, **5-DON**, or **10-DON**, respectively, which were assembled under standard conditions and characterized by gel electrophoresis and AFM (see Figure S1 in the Supporting Information). We initially investigated how the length of the double helix formed upon hybridization between DONs and surface-bound capture strands affects the efficacy of DON immobilization (Figure 1C,D). To this end, arrays of capture oligonucleotides of different lengths (F1, F5, F10, 3–22 nt) were prepared by ink-jet printing on chemically activated glass surfaces[13] and Cy3-labeled DONs were allowed to hybridize. Fluorescent signals with a high signal-to-noise ratio exclusively occurred on the spots encoded with the complementary capture oligonucleotides as a clear indication for highly specific binding (see also Figures S2–S5).

The length of capture oligomers significantly affected the hybridization efficacy of the DON (Figure 1D). Interestingly, the three different capture systems F1, F5, and F10 revealed distinctively different and highly reproducible profiles of length-dependent binding (Figure S3). These sequence-specific profiles were slightly affected by the hybridization temperature (25 or 45 °C, see Figure S4) and most likely correlate with the formation of secondary structures in the single-stranded binding sites of the DONs and/or capture oligomers (Figure S5). Since the 12-mer capture oligomers of the three different sequences revealed similar hybridization efficacy, this particular length was used for all further studies. As expected, reducing the number of binding sites tethered to the DONs led to a decrease in surface binding (Figure S6). Furthermore, the site-specific sorting of a mixture of two differently labeled origami constructs, **1-DON^{Cy3}** and **5-DON^{Cy5}**, also worked perfectly fine with microarrays of smaller capture features (ca. 5 μm diameter) prepared by polymer-pen lithography (PPL)[14,15] (Figure 1B) instead of ink-jet printing (ca. 150–200 μm diameter spots).

We then investigated the site-selective immobilization of protein-loaded DONs on DNA microarrays. To this end, we initially assembled Cy5-labeled **1-DON** variants which contained either 3 or 15 biotinylated staples (**DON^{Cy5}-b$_3$**, **1-DON^{Cy5}-b$_{15}$**) to facilitate the binding of Cy3-labeled streptavidin (STV) molecules (Figure 2A, see also Figure S7). The resulting constructs, **1-DON^{Cy5}**, **1-DON^{Cy5}-STV$_3$**, and **1-DON^{Cy5}-STV$_{15}$** were allowed to bind to microarrays which contained 100 spots of the complementary F1$_{12}$ and, as control for specific binding, 40 spots of the non-complementary F9 capture (Figure 2B). An additional control, in which the Cy3-labeled STV was blocked with free biotin prior to binding to the **1-DON-b$_{15}$** proved that no non-specific binding occurred in this experiment (array IV, in Figure 2B). Indeed, exclusively site-specific binding was clearly evident from the observed Cy3 signals. As detectable from the Cy5 signals, attachment of STV molecules led to slight decrease in origami binding, as compared to unmodified DONs. We speculate that the decrease might stem from electrostatic or steric repulsion between the protein-decorated origami structure and the solid surface. The efficient sorting of protein-loaded constructs was further demonstrated in a three-color experiment using a mixture of three different DONs (**1-DON**, **5-DON**, or **10-DON**) each loaded with 15 differently fluorescence-labeled STV molecules (Cy3, Cy5, FAM, respectively, Figure 2C). We also demonstrated the accessibility and functionality of surface-immobilized STV-loaded **1-DON^{Cy5}-b$_{15}$** constructs through binding of biotinylated immunoglobulin G (IgG) molecules and detection with a Cy3-labeled secondary antibody (Figure 2D, see also Figure S8). All these experiments clearly indicated that the DNA-directed immobilization of protein-decorated origami nanostructures functioned well with exquisite site selectivity.

We then carried out a proof-of-concept study to demonstrate that the microarray-immobilized DONs can be applied as an interface to study membrane-associated processes in living cells. We used origami constructs presenting the epidermal growth factor (EGF) as ligand to activate the cellular epidermal growth factor receptor (EGFR) in adhered MCF7 cells. A series of Cy3-labeled **1-DON** constructs was decorated with either 4, 5, 8, or 12 STV molecules which also varied in their nanoscaled architecture (Figure 3). Specifically, the STV molecules were either arranged evenly distributed ("far") or densely clustered ("close") on the surface of the origami structure, as indicated by the schematic illustration and AFM images of the constructs **1-DON-4f**, **1-DON-5f**, **1-DON-8f**, **1-DON-12f**, or **1-DON-4c**, **1-DON-5c**, **1-DON-8c**, **1-DON-12c**, respectively, in Figure 3. The various DON constructs revealed comparable surface occupancies with STV molecules and hybridization efficacies (Figures S9, S10). After coupling biotinylated EGF to the constructs, they were immobilized on PPL microarrays bearing dense patterns of the F1$_{12}$ capture oligomer (spot size ca. 5 μm diameter).

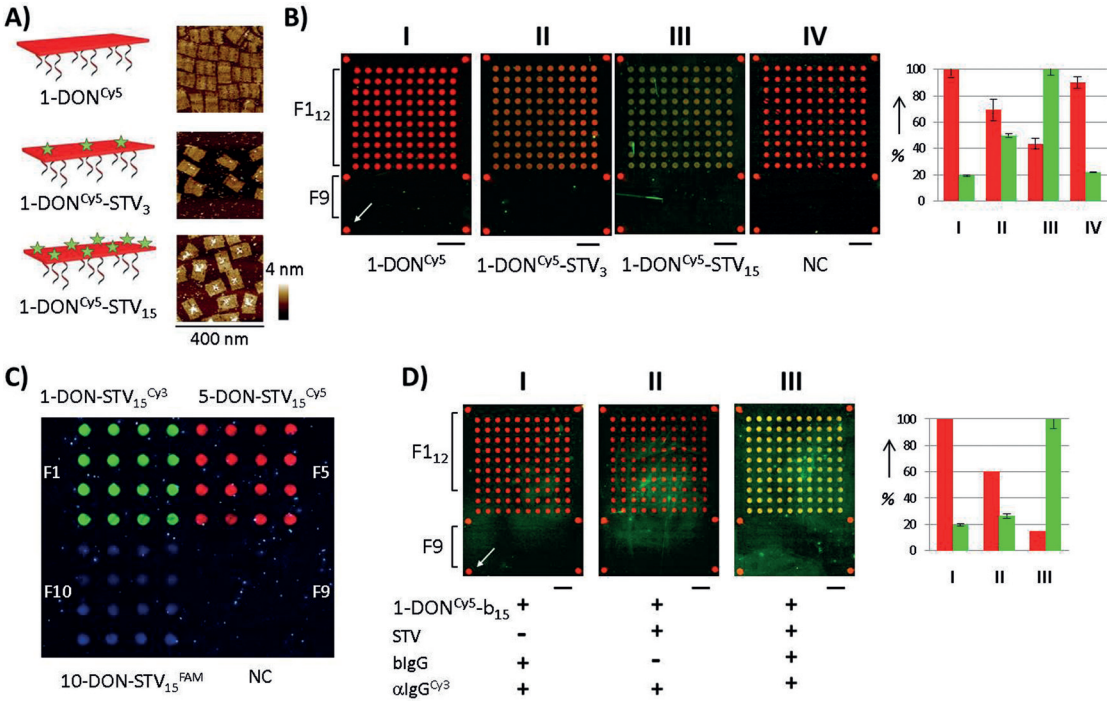

Figure 2. Immobilization of protein-loaded DONs. A) Schematic illustration of DON designs with respective AFM images. B) Immobilization of Cy5-labeled **1-DON^{Cy5}** (red) containing different numbers of Cy3-labeled STV (green; NC = negative control in which the Cy3-labeled STV was blocked with biotin prior to incubation with **1-DON^{Cy5}-b$_{15}$**). Mean fluorescent signals of the arrays, normalized against Cy5 reference spots (white arrow), are shown in the histograms. All arrays contained 40 control spots with non-complementary capture F9 (bottom) in addition to the complementary F1$_{12}$ capture (top). C) Sorting of a mixture of three different DONs, each loaded with 15 differently labeled STV molecules, on a microarray containing 4×4 spots (ca. 200 μm diameter) of three complementary (F1, F5, F10) and one non-complementary (F9) capture oligomer. D) STV-loaded **1-DON^{Cy5}-b$_{15}$** (red) was immobilized on F1 microarrays (configured as in B) and coupled with biotinylated IgG (bIgG). Bound bIgG was detected with a Cy3-labeled *anti*-IgG antibody (αIgG^{Cy3}, green). Arrays I and II are controls in which either the STV or the bIgG was omitted, respectively. Normalized mean fluorescent signals and standard deviations are shown in the histograms. As indicated by the Cy5 signals (red bars in B and D), protein loading and washing steps decrease the amount of immobilized origami construct.

Owing to their Cy3-labels, the immobilized constructs were visible as regular patterns by fluorescence microscopy in the green channel (image II, in Figure 3). Human MCF7 cells expressing the EGF receptor genetically fused to enhanced green fluorescent protein (eGFP-EGFR) were then allowed to adhere on those surfaces for 45 minutes. After fixation, the cells were clearly visible by their eGFP fluorescence (violet channel, image IV in Figure 3) and DAPI-stained nuclei (blue channel, image V). Activated EGFR is phosphorylated at tyrosine 1068, which was detected by staining with a specific Cy5-labeled antibody, visible in the red channel (image III). Visual inspection of the fluorescence micrographs clearly revealed activated EGFR (red) features co-localized with the immobilized **1-DON** (green) features (image I, see also Figure S11 in the Supporting Information).

To analyze whether the nanostructural features of the immobilized EGF-DONs affect the activation of EGFR in the adhered MCF7 cells, we carried out a statistical analysis where the average numbers of red spots underneath an adhered cell were determined for the eight different DON constructs (Figure 3, for statistical details, see also Table S1, Supporting Information). The obtained box-whisker plots clearly indicate that both stoichiometry and spatial arrangement of the DON-EGF constructs quantitatively influence EGFR activation. While no activation occurred in the absence of EGF-STV entities on the origami structure or the presence of free, soluble EGF in the medium (Figure S11), increasing numbers of ligands led to an increased activation, which leveled off at eight ligands per origami construct. In the case of 4 or 5 EGF-STV entities per DON, constructs with evenly distributed ("far") ligands revealed a significant larger receptor activation than their complementary analogs, containing the same number of ligands in densely clustered ("close") arrangements. This effect of the spatial distribution of the ligand was less pronounced with 8 and with 12 ligands per origami construct (see also Figure S12).

Taking into account the size of the 53 amino acid EGF ligand and the presence of an about 1 nm spacer between EGF and the biotin, we estimate that a single EGF-STV entity on the surface of the origami construct typically contains two–three molecules of EGF. Hence, each entity should be capable to bind two EGFR molecules in the plasma membrane of the cell, such that EGFR dimerization can occur to enable ligand-induced EGFR autophosphorylation.[16,17] Since the uncertainty in the relative EGF-to-STV stoichiometry is averaged out in all the experiments shown in Figure 3, it cannot be responsible for the observed differences between low numbers of distributed or clustered ligand entities (e.g., **1-DON-4f** vs. **1-DON-4c,** or **1-DON-5f** vs. **1-DON-5c**). Instead, many different biological processes could account for the observed differences. These include a restricted availability of EGFR in the plasma membrane because of limited local

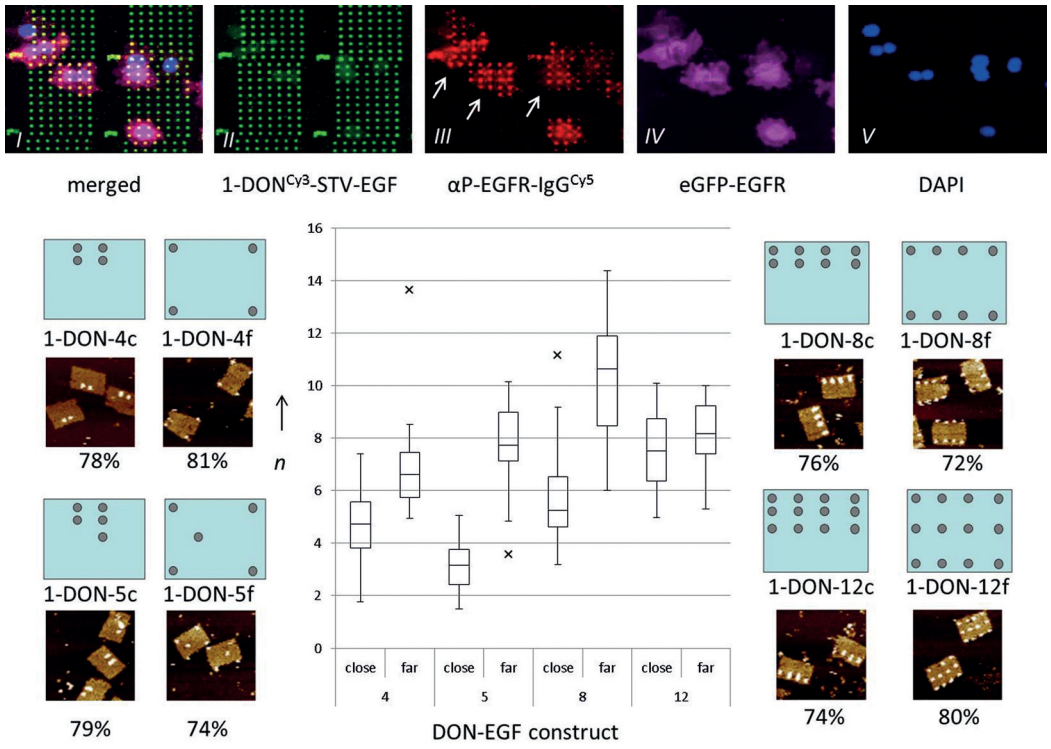

Figure 3. The nanostructural features of MOSAIC affect the response of adhered MCF7 cells. A series of Cy3-labeled **1-DON** constructs was prepared decorated with different numbers and arrangements of EGF-modified STV entities, as indicated by the schemes and corresponding AFM images (250×250 nm^2 scans, average surface occupancies of the DONs with STV molecules listed underneath, see also Figure S9). The constructs were immobilized on DNA microarrays, thus leading to the 5 μm spot patterns, visible in image II of the upper row of fluorescence micrographs, obtained from experiments with construct **1-DON-5 f**. MCF7 cells expressing an eGFP-tagged EGF receptor (eGFP-EGFR) were allowed to adhere to the patterned DON surfaces and then fixed. The fluorescence of eGFP-EGFR and DAPI staining (images IV and V, respectively) allows one to identify individual cells. Activated EGFR was detected by staining with a specific Cy5-labeled antibody (αP-EGFR^{Cy5}), visible as red spots (marked by white arrows in image III). The average numbers of red spots underneath an adhered cell, determined for the eight different EGF-DON constructs are indicated as box-whisker-plot histograms (see also Figures S11, S12). Note that all constructs with evenly distributed ("far") EGF-STV entities lead to a larger receptor activation than their complementary analogs, containing densely clustered ("close") arrangements of the same number of ligands.

concentrations and lateral diffusion, geometric constraints originating from specific arrangements of EGFR with the actin cytoskeleton, biochemical factors originating from components of downstream signaling, receptor internalization, or others. While our initial findings call for in-depth studies to unravel the biological response mechanisms, the here presented results clearly demonstrate that a) the surface-patterns of EGF-decorated DONs were stable under cell culture conditions, b) the presented ligands were able to bind to and activate their cognate EGF receptor, and c) the ligand architecture at the nanometer length scale influences the response of the adhered cells.

In conclusion, we here demonstrated for the first time the site-directed sorting of differently encoded, protein-decorated DNA origami structures on DNA microarrays. The combination of bottom-up self-assembly of protein–DNA nanostructures and top-down micropatterning of solid surfaces enabled the creation of multiscale origami structures as interface for cells (MOSAIC). In a first proof-of-concept, we applied this technology to investigate the activation of EGF receptors in living MCF7 cells through distinctive nanoscale arrangements of EGF ligands. We believe that MOSAIC has significant advantages over conventional techniques for the study of ligand-induced receptor processes, such as the use of surfaces patterned with supported bilayer patches and nanoscaled mobility barriers to present geometrically constrained ligands to adhered cells.[7,18] Since these approaches have limited lateral resolution and multiplexing capabilities, they cannot control the absolute number, stoichiometry, and precise nanoscale orientation of different ligands. While arranging various ligands with distances in the critical range of biomolecular assemblies (ca. 5–100 nm) has been achieved with soluble DNA-tethered ligand dimers and trimers to affect transmembrane receptors,[19] these soluble assemblies do not offer the advantages of surface-based techniques: the rational tailoring of nano-to-microscale geometries and the implementation of multiplexed high-throughput applications. MOSAIC combines the advantages of the two complementary approaches. We believe that further miniaturization of the encoded surface patterns (e.g., by AFM nanografting)[20] and/or the assembly of larger origami structures,[21] will even enable to fully control absolute numbers and nanoscale architecture of ligands on surfaces.[22] Furthermore, the refinement of effective protein–DNA conjugation chemistries[6c] and the implementation of microfluidic techniques to enable simultaneous manipulation and analysis of cultured cells[23] will deploy the full potential of MOSAIC to create artificial biointerfaces useful to explore and exploit basic processes of cellular signaling and communication.

Acknowledgements

We gratefully acknowledge financial support of this work by Deutsche Forschungsgemeinschaft (grant number NI 399/10-

2) and the Helmholtz programme BioInterfaces in Technology and Medicine. This work was partly carried out with the support of the Karlsruhe Nano Micro Facility (KNMF), a Helmholtz Research Infrastructure at KIT. We thank Katja Koßmann, Ann-Kathrin Schneider, and Cornelia Ziegler for experimental help, Nicholas S. Foulkes, Olivier Kassel, Pavel Nikolov, and Tim Scharnweber for fruitful discussions on the project, and Pedro Roda-Navarro (MPI Dortmund) for supplying the stable eGFP-EGFR MCF-7 cell line expressing eGFP-tagged Erbb1 receptors.

Keywords: cell cultures · DNA · nanostructures · proteins · surface chemistry

How to cite: *Angew. Chem. Int. Ed.* **2015**, *54*, 15813–15817
Angew. Chem. **2015**, *127*, 16039–16043

[1] Reviews: a) M. C. Pirrung, *Angew. Chem. Int. Ed.* **2002**, *41*, 1276; *Angew. Chem.* **2002**, *114*, 1326; b) J. Sobek, K. Bartscherer, A. Jacob, J. D. Hoheisel, P. Angenendt, *Comb. Chem. High Throughput Screening* **2006**, *9*, 365; c) A. Sassolas, B. D. Leca-Bouvier, L. J. Blum, *Chem. Rev.* **2008**, *108*, 109; d) P. Baldi, G. W. Hatfield, *DNA Microarrays and Gene Expression: From Experiments to Data Analysis and Modeling*, Cambridge University Press, Cambridge, **2011**.

[2] Reviews: a) D. S. Yeo, R. C. Panicker, L. P. Tan, S. Q. Yao, *Comb. Chem. High Throughput Screening* **2004**, *7*, 213; b) P. Jonkheijm, D. Weinrich, H. Schroeder, C. M. Niemeyer, H. Waldmann, *Angew. Chem. Int. Ed.* **2008**, *47*, 9618; *Angew. Chem.* **2008**, *120*, 9762; c) D. Weinrich, P. Jonkheijm, C. M. Niemeyer, H. Waldmann, *Angew. Chem. Int. Ed.* **2009**, *48*, 7744; *Angew. Chem.* **2009**, *121*, 7880; d) Y. M. Foong, J. Fu, S. Q. Yao, M. Uttamchandani, *Curr. Opin. Chem. Biol.* **2012**, *16*, 234; e) H. Sun, G. Y. Chen, S. Q. Yao, *Chem. Biol.* **2013**, *20*, 685.

[3] Examples: a) R. C. Bailey, G. A. Kwong, C. G. Radu, O. N. Witte, J. R. Heath, *J. Am. Chem. Soc.* **2007**, *129*, 1959; b) H. Schroeder, B. Ellinger, C. F. W. Becker, H. Waldmann, C. M. Niemeyer, *Angew. Chem. Int. Ed.* **2007**, *46*, 4180–4183; *Angew. Chem.* **2007**, *119*, 4258–4261; c) S. Gandor, S. Reisewitz, M. Venkatachalapathy, G. Arrabito, M. Reibner, H. Schroder, K. Ruf, C. M. Niemeyer, P. I. Bastiaens, L. Dehmelt, *Angew. Chem. Int. Ed.* **2013**, *52*, 4790; *Angew. Chem.* **2013**, *125*, 4890; d) for a recent review, see: R. Meyer, S. Giselbrecht, B. E. Rapp, M. Hirtz, C. M. Niemeyer, *Curr. Opin. Chem. Biol.* **2014**, *18C*, 8.

[4] N. C. Seeman, *Nature* **2003**, *421*, 427.

[5] P. W. Rothemund, *Nature* **2006**, *440*, 297.

[6] Reviews: a) W. M. Shih, C. Lin, *Curr. Opin. Struct. Biol.* **2010**, *20*, 276; b) J. Nangreave, D. Han, Y. Liu, H. Yan, *Curr. Opin. Chem. Biol.* **2010**, *14*, 608; c) C. M. Niemeyer, *Angew. Chem. Int. Ed.* **2010**, *49*, 1200; *Angew. Chem.* **2010**, *122*, 1220; d) A. M. Hung, H. Noh, J. N. Cha, *Nanoscale* **2010**, *2*, 2530; e) T. Tørring, N. V. Voigt, J. Nangreave, H. Yan, K. V. Gothelf, *Chem. Soc. Rev.* **2011**, *40*, 5636; f) B. Saccà, C. M. Niemeyer, *Angew. Chem. Int. Ed.* **2012**, *51*, 58; *Angew. Chem.* **2012**, *124*, 60; g) F. C. Simmel, *Curr. Opin. Biotechnol.* **2012**, *23*, 516; h) Q. Liu, C. Song, Z. G. Wang, N. Li, B. Ding, *Methods* **2014**, *67*, 205; i) J. Fu, M. Liu, Y. Liu, H. Yan, *Acc. Chem. Res.* **2012**, *45*, 1215.

[7] N. C. Hartman, J. T. Groves, *Curr. Opin. Cell Biol.* **2011**, *23*, 370.

[8] a) A. E. Gerdon, S. S. Oh, K. Hsieh, Y. Ke, H. Yan, H. T. Soh, *Small* **2009**, *5*, 1942; b) J. M. Yun, K. N. Kim, J. Y. Kim, D. O. Shin, W. J. Lee, S. H. Lee, M. Lieberman, S. O. Kim, *Angew. Chem. Int. Ed.* **2012**, *51*, 912; *Angew. Chem.* **2012**, *124*, 936; c) A. C. Pearson, E. Pound, A. T. Woolley, M. R. Linford, J. N. Harb, R. C. Davis, *Nano Lett.* **2011**, *11*, 1981; d) M. Pillers, V. Goss, M. Lieberman, *Acc. Chem. Res.* **2014**, *47*, 1759.

[9] a) R. J. Kershner, L. D. Bozano, C. M. Micheel, A. M. Hung, A. R. Fornof, J. N. Cha, C. T. Rettner, M. Bersani, J. Frommer, P. W. Rothemund, G. M. Wallraff, *Nat. Nanotechnol.* **2009**, *4*, 557; b) A. M. Hung, C. M. Micheel, L. D. Bozano, L. W. Osterbur, G. M. Wallraff, J. N. Cha, *Nat. Nanotechnol.* **2010**, *5*, 121; c) T. Akishiba, N. Tamura, T. Ichii, Y. Hirai, K. Sugano, T. Tsuchiya, H. Sugimura, O. Tabata in *Micro Electro Mechanical Systems (MEMS)*, *IEEE 26th International Conference*, Taipei, Taiwan, **2013**; d) M. B. Scheible, G. Pardatscher, A. Kuzyk, F. C. Simmel, *Nano Lett.* **2014**, *14*, 1627.

[10] a) M. Langecker, V. Arnaut, J. List, F. C. Simmel, *Acc. Chem. Res.* **2014**, *47*, 1807; b) Y. Suzuki, M. Endo, Y. Yang, H. Sugiyama, *J. Am. Chem. Soc.* **2014**, *136*, 1714; c) S. Kocabey, S. Kempter, J. List, Y. Xing, W. Bae, D. Schiffels, W. M. Shih, F. C. Simmel, T. Liedl, *ACS Nano* **2015**, *9*, 3530.

[11] M. Erkelenz, D. M. Bauer, R. Meyer, C. Gatsogiannis, S. Raunser, B. Sacca, C. M. Niemeyer, *Small* **2014**, *10*, 73.

[12] U. Feldkamp, R. Wacker, W. Banzhaf, C. M. Niemeyer, *ChemPhysChem* **2004**, *5*, 367.

[13] S. Reisewitz, H. Schroeder, N. Tort, K. A. Edwards, A. J. Baeumner, C. M. Niemeyer, *Small* **2010**, *6*, 2162.

[14] F. Brinkmann, M. Hirtz, A. M. Greiner, M. Weschenfelder, B. Waterkotte, M. Bastmeyer, H. Fuchs, *Small* **2013**, *9*, 3266.

[15] G. Arrabito, H. Schroeder, K. Schroder, C. Filips, U. Marggraf, C. Dopp, M. Venkatachalapathy, L. Dehmelt, P. I. Bastiaens, A. Neyer, C. M. Niemeyer, *Small* **2014**, *10*, 2870.

[16] I. Chung, R. Akita, R. Vandlen, D. Toomre, J. Schlessinger, I. Mellman, *Nature* **2010**, *464*, 783.

[17] S. Doumiati, K. Haupt, C. Rossi, *J. Mol. Recognit.* **2012**, *25*, 623.

[18] a) A. J. Torres, M. Wu, D. Holowka, B. Baird, *Annu. Rev. Biophys.* **2008**, *37*, 265; b) P. M. Nair, K. Salaita, R. S. Petit, J. T. Groves, *Nat. Protoc.* **2011**, *6*, 523; c) A. C. Greene, S. J. Lord, A. Tian, C. Rhodes, H. Kai, J. T. Groves, *Biophys. J.* **2014**, *106*, 2196.

[19] a) J. M. Paar, N. T. Harris, D. Holowka, B. Baird, *J. Immunol.* **2002**, *169*, 856; b) D. Sil, J. B. Lee, D. Luo, D. Holowka, B. Baird, *ACS Chem. Biol.* **2007**, *2*, 674; c) A. Shaw, V. Lundin, E. Petrova, F. Fordos, E. Benson, A. Al-Amin, A. Herland, A. Blokzijl, B. Hogberg, A. I. Teixeira, *Nat. Methods* **2014**, *11*, 841.

[20] F. Bano, L. Fruk, B. Sanavio, M. Glettenberg, L. Casalis, C. M. Niemeyer, G. Scoles, *Nano Lett.* **2009**, *9*, 2614.

[21] A. N. Marchi, I. Saaem, B. N. Vogen, S. Brown, T. H. LaBean, *Nano Lett.* **2014**, *14*, 5740.

[22] The density of capture oligonucleotides and immobilized DONs were estimated by aid of ink-jet deposition of known amounts of fluorescence-labeled oligonucleotides (G. Arrabito, S. Reisewitz, L. Dehmelt, P. I. Bastiaens, B. Pignataro, H. Schroeder, C. M. Niemeyer, *Small* **2013**, *9*, 4243). This led to surface densities of about 10000 capture oligomers and 10–20 origami structures per square-micrometer. Taking into account the 25 μm^2 area of a typical PPL microspot used in the cell experiments (Figure 3), we estimate that 250–500 origami structures are deposited in a single spot with an average distance of about 150 nm among the individual origami plates (Figure S13). The typical distances among the EGF-STV ligand sites on each origami structures vary from 5–80 nm, depending on the DON design (Figure S13). Further mechanistic studies, which include systematic variations of different origami configurations, ligand numbers, as well as DON surface densities are underway to unravel the biological response to the nanostructural features of this MOSAIC system.

[23] M. Mehling, S. Tay, *Curr. Opin. Biotechnol.* **2014**, *25*, 95.

Received: October 19, 2015
Revised: November 12, 2015
Published online: December 7, 2015

